One-equation near-wall turbulence modeling with the aid of direct simulation data

By W. Rodi[1] AND N. N. Mansour[2]

The length scales appearing in the relations for the eddy viscosity and dissipation rate in one-equation models were evaluated from direct numerical simulation data for developed channel and boundary-layer flow at two Reynolds numbers each. To prepare the ground for the evaluation, the distribution of the most relevant mean-flow and turbulence quantities is presented and discussed, also with respect to Reynolds-number influence and to differences between channel and boundary-layer flow. An alternative model is also examined in which $(\overline{v'^2})^{1/2}$ is used as velocity scale instead of $k^{1/2}$. With this velocity scale, the length scales now appearing in the model follow very closely a linear relationship near the wall so that no damping is necessary. For the determination of $\overline{v'^2}$ in the context of a one-equation model, a correlation is provided between $\overline{v'^2}/k$ and $\overline{u'v'}/k$.

1. Introduction

One-equation eddy-viscosity models have recently regained popularity as components of two-layer turbulence models (see *e.g.* Rodi, 1991). In these, one-equation models are used only near walls in the viscosity-affected region, say up to wall distances where the ratio of eddy viscosity to molecular viscosity takes values of 20 to 40, which corresponds to wall distances of up to $y^+ \approx 80$ in boundary-layer flow. Outside this near-wall region, other, more general models are employed such as the two-equation k-ϵ model or Reynolds-stress-equation models.

In existing one-equation models, the local state of the turbulence is characterized by the velocity scale $k^{1/2}$ and the length scale l. The turbulent kinetic energy k is calculated from a transport equation, while the l-distribution is prescribed empirically. In attached near-wall flows, the only Reynolds stress of importance in the momentum equations is the shear stress $-\overline{u'v'}$, which is determined from the eddy-viscosity relation

$$-\overline{u'v'} = \nu_t U_{,y} \tag{1}$$

In one-equation models, the eddy viscosity is calculated from

$$\nu_t = C_\mu k^{1/2} l_\mu \tag{2}$$

1 University of Karlsruhe, F. R. Germany
2 NASA Ames Research Center

and the distribution of k from the following transport equation for k:

$$Uk_{,x} + Vk_{,y} = \left[\left(\nu + \frac{\nu_k}{\sigma_k}\right) k_{,y}\right] - \overline{u'v'}U_{,y} - \epsilon \tag{3}$$

The dissipation rate ϵ appearing in this equation is determined from

$$\epsilon = k^{3/2}/l_\epsilon \tag{4}$$

When the coefficient C_μ in (2) is chosen as the square of the structure parameter $\overline{u'v'}/k$ under local equilibrium conditions, the length scales l_μ and l_ϵ are the same in the log-law region, but they may differ very close to the wall. They are usually prescribed empirically by formulae of the following type

$$l_\mu = C_l y(1 - \exp(-y^*/A_\mu^*)) \tag{5}$$

$$l_\epsilon = C_l y(1 - \exp(-y^*/A_\epsilon^*)) \tag{6}$$

where

$$y^* = k^{1/2}y/\nu \tag{7}$$

and A_μ^* and A_ϵ^* are empirical constants. Hence, the length scales basically increase linearly with distance from the wall at the same rate, but their magnitude is reduced near the wall by exponential damping functions, which are similar to the van Driest damping function in the mixing-length model and are different for l_μ and l_ϵ. This is basically the model due to Wolfshtein (1969), while Norris and Reynolds (1975) used a function $(1 + C_\epsilon y^*)^{-1}$ to damp the dissipation scale l_ϵ near the wall. Of course, the length scales grow linearly only near the wall; altogether a ramp function is assumed with a uniform l-distribution in the outer part of the flow. However, in this paper we are concerned only with the near-wall region. The argument in the damping functions is taken as $y^* = k^{1/2}y/\nu$ and not $y^+ = U_\tau y/\nu$ because the functions should also work for separated flows where U_τ can go to zero.

The length-scale prescriptions (5) and (6) are based on compatibility with the universal logarithmic velocity distribution and lean heavily on experience with the mixing-length distribution near the wall, *i.e.* on the van Driest damping law. So far, the validity of the prescriptions could not be checked directly with the aid of data but only indirectly through their use in flow calculations. Direct numerical simulation (DNS) data are now available to test the length-scale relations directly and to form the basis for developing improved prescriptions if necessary. To this end, l_μ- and l_ϵ-distributions are calculated in this paper from DNS data for developed channel (Kim *et al.*, 1987 and Kim, 1990) and boundary-layer (Spalart, 1988) flows at two Reynolds numbers each, and these data are compared with the existing empirical relations. The influence of the Reynolds number is thereby also examined. Alternative modeling with the normal fluctuations $(\overline{v'^2})^{1/2}$ as velocity scale instead of $k^{1/2}$ is also investigated, and $\overline{v'^2}/k$ is correlated with $\overline{u'v'}/k$ so that no extra equation need be solved for $\overline{v'^2}$ and the one-equation-model character is retained.

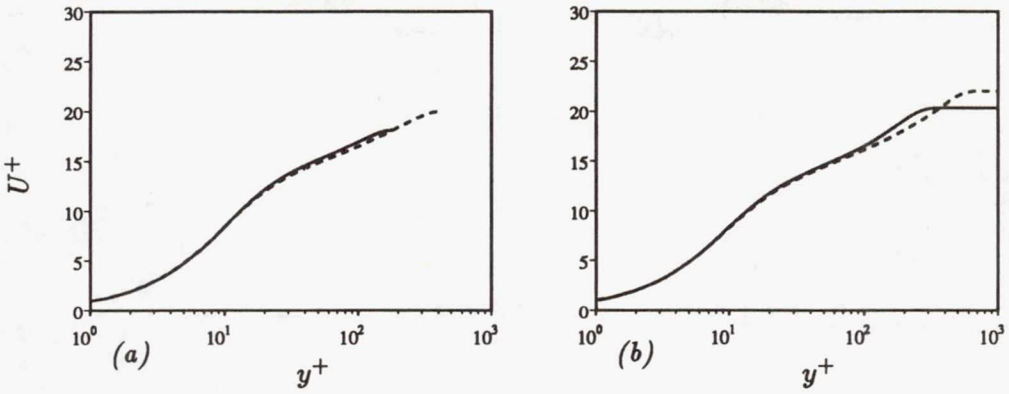

FIGURE 1. Velocity profiles in wall coordinates.
(a) Channel: —— $Re_\tau = 180$; ---- $Re_\tau = 395$.
(b) Boundary layer: —— $Re_\theta = 670$; ---- $Re_\theta = 1416$.

2. Basic quantities needed for model evaluation

The ground for the model evaluation needs to be prepared first by providing distributions of basic quantities in channel flow and boundary layers as computed from the DNS data. Here, the influence of the Reynolds number and of the flow situation (channel flow versus boundary layer) is examined with the quantities plotted in wall coordinates, *i.e.* they are made dimensionless with U_τ and ν. As components of two-layer models, one-equation models are mostly used for globally high-Reynolds-number situations and hence the model relations should correspond closely to such situations; the tuning of the model to data stemming from rather low Reynolds-number flows is therefore not desirable. Hence, it is important to examine how closely the DNS data obtained for the highest Reynolds numbers correspond to experimental data achieved at high Reynolds numbers.

All quantities to be presented in the following are made dimensionless with the friction velocity U_τ and with ν, and they are plotted against $y^+ = U_\tau y/\nu$. First, the velocity distribution is given in the usual semi-log plot in Fig. 1. For channel flow (Fig. 1a), there appears to be a reasonably well established log law for both Reynolds numbers, but for the lower Reynolds number ($Re_\tau = 180$) the constant C in the log law is above the standard value 5, while for $Re_\tau = 395$ the velocity distribution follows the standard log law over a significant part of the channel half-width. At fairly low Reynolds numbers, the increase in the log-law constant C with decreasing Reynolds number is a well known phenomenon (see *e.g.* Launder, 1986). For the boundary layer at the lower Reynolds number ($Re_\theta = 667$), the velocity distribution follows the log law in a small region only, while at the higher Reynolds number ($Re_\theta = 1416$) this region is fairly extensive (up to nearly $y^+ \approx 100$). For both channel and boundary-layer flows, the von Kármán constant derived from the data is $\kappa = 0.41$. Hence, in the higher-Reynolds-number cases, the velocity distribution corresponds to the observed distribution at much higher Reynolds numbers over a significant portion of the flow. The deviation from the log

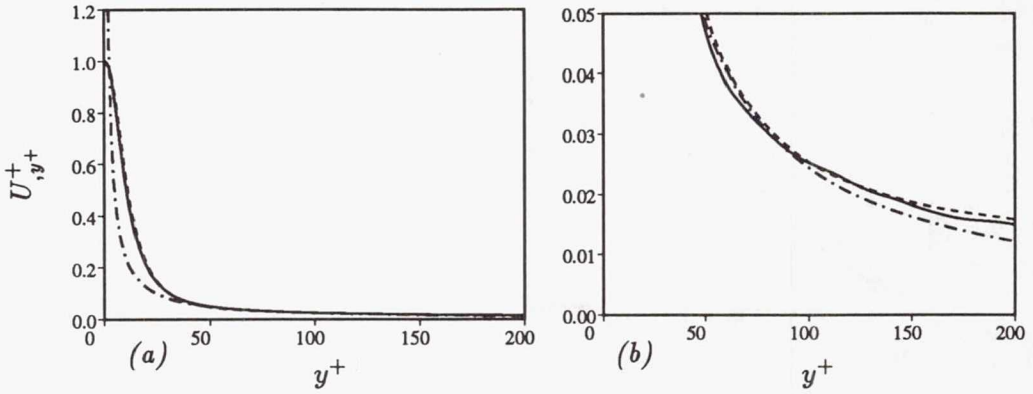

FIGURE 2. Distribution of velocity gradient. —— Channel $Re_\tau = 395$; ---- Boundary layer $Re_\theta = 1416$; —·— $1/.41y^+$. *(a)* Vertical scale between 0 and 1.2. *(b)* Expanded vertical scale between 0. and 0.05.

law can be seen more clearly in Fig. 2 where the velocity gradient $U^+_{,y^+}$ is plotted. According to the log law this gradient should follow the curve $1/\kappa y^+$, Fig. 2 shows that for both higher-Reynolds-number flows (channel flow and boundary layer) the velocity gradient starts to deviate from this curve at $y^+ \approx 30$.

Fig. 3 shows for channel flow the distribution of the RMS values of the fluctuating velocity components u, v and w compared with measurements of various experiments at high Reynolds numbers, as compiled by Myong and Kasagi (1988). The measurements show considerable scatter, and extreme data points should not be considered trustworthy. The DNS data exhibit a surprising dependence on the Reynolds number even close to the wall, particularly so for the component w. However, there is a clear trend with increasing Reynolds number towards the mean of the experimental data, and the DNS data for $Re_\tau = 395$ are already a fairly good representation of the high-Reynolds-number experimental data. Hence it may be concluded that the higher-Re channel flow data correspond closely to high-Re channel flow for which the quantities considered are independent of Reynolds number. In Fig. 4, the corresponding DNS data for the boundary layer are presented at two Reynolds numbers. Here a similar Re-dependence is found, and it is interesting to note that, except very close to the wall, the fluctuating velocities in the boundary layer are somewhat higher than in the channel flow. This may be due partly to the differences in the flow situation with the shear stress $-\overline{u'v'}$ falling more quickly with distance from the wall in the channel flow than in the boundary layer, but to some extent it is also due to the fact that the boundary-layer flow at $Re_\theta = 1416$ represents a higher Reynolds-number case than the channel flow at $Re_\tau = 395$. This can be inferred from the higher y^+- and ν_t/ν-values in the boundary layer (see Figs. 1 and 9).

The ratios $\overline{u'^2}/k$, $\overline{v'^2}/k$ and $\overline{w'^2}/k$ needed in section 4 are shown for both flows in Fig. 5. Up to $y^+ \approx 100$, there is generally little influence of the Reynolds number on these ratios, and there is also fairly good agreement between channel

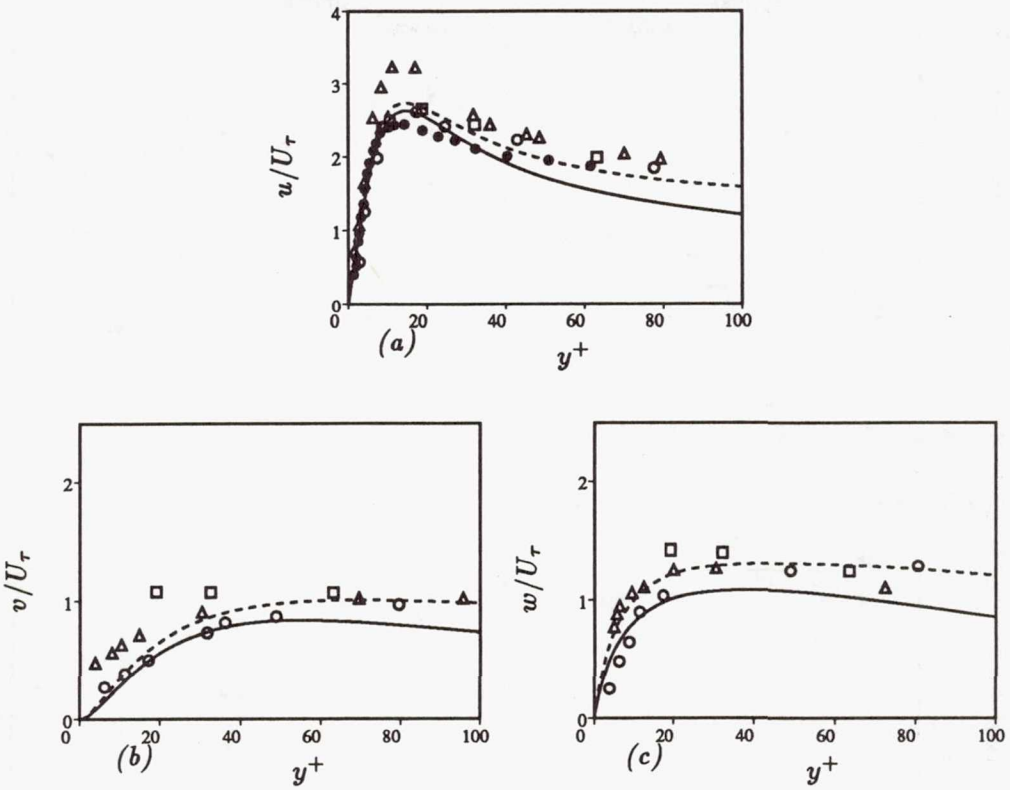

FIGURE 3. RMS fluctuations in developed channel flow, comparison with high-Reynolds-number data compiled by Myong and Kasagi (1988). —— DNS, $Re_\tau = 180$; ---- DNS, $Re_\tau = 395$; ○ Laufer (1954), $Re = 50,000$; △ Clark (1968), $Re = 30,400$; □ Kastrinakis & Eckelmann (1983), $Re = 25,200$; • Hussain & Reynolds (1975), $Re = 27,600$.

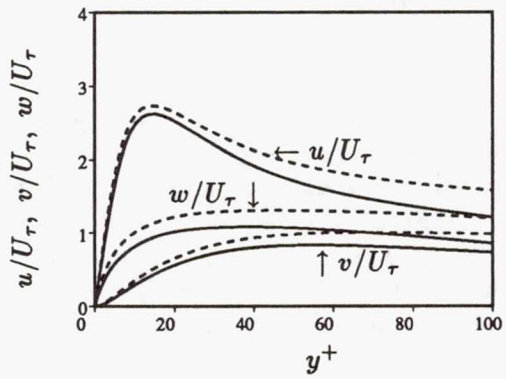

FIGURE 4. RMS fluctuations in boundary layers. —— $Re_\theta = 667$; ---- $Re_\theta = 1416$.

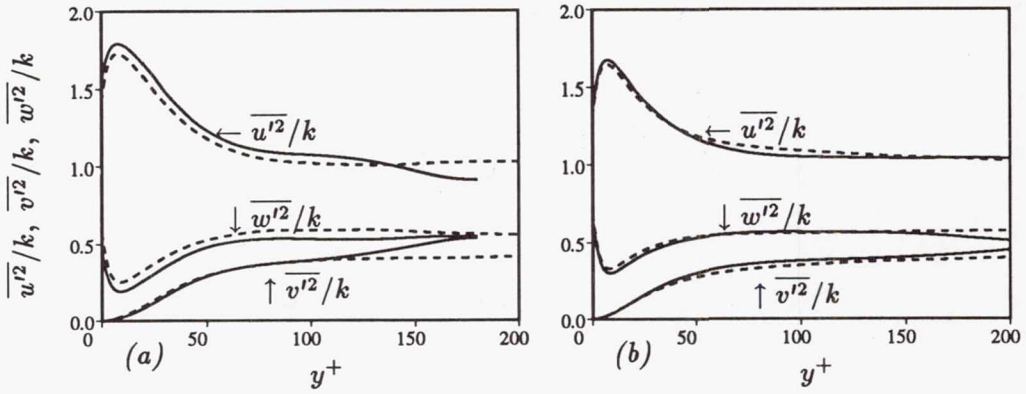

FIGURE 5. Distribution of $\overline{u'^2}/k$, $\overline{v'^2}/k$, $\overline{w'^2}/k$.
(a) Channel: —— $Re_\tau = 180$; ---- $Re_\tau = 395$.
(b) Boundary layer: —— $Re_\theta = 670$; ---- $Re_\theta = 1416$.

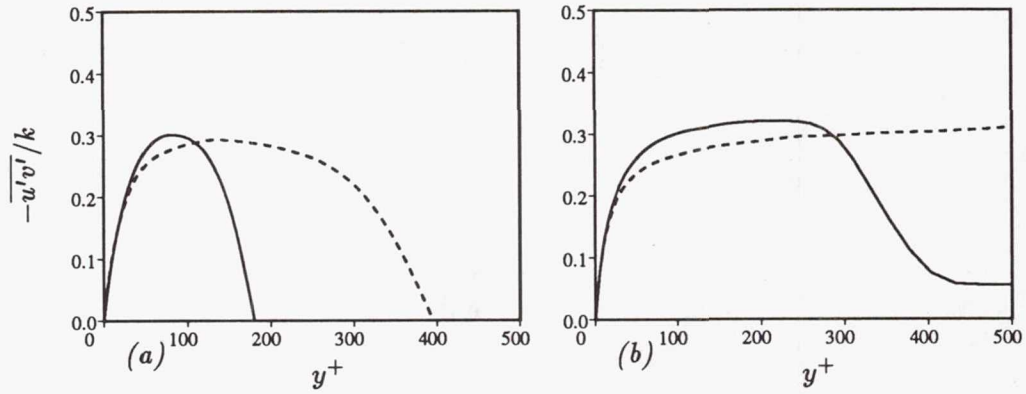

FIGURE 6. Distribution of structure parameter $-\overline{u'v'}/k$.
(a) Channel: —— $Re_\tau = 180$; ---- $Re_\tau = 395$.
(b) Boundary layer: —— $Re_\theta = 670$; ---- $Re_\theta = 1416$.

and boundary-layer flow. An exception is $\overline{w'^2}/k$, which has a larger dip near the wall in the channel-flow case. For the higher-Reynolds-number cases, constant values are a reasonable approximation to the data for $y^+ \geq 80$, with $\overline{u'^2}/k \approx 1$, $\overline{v'^2}/k \approx .41$ and $\overline{w'^2}/k \approx 0.59$. The distribution of the structure parameter $-\overline{u'v'}/k$ is given in Fig. 6. For the channel flow, the range where this parameter assumes approximately the standard value of 0.3 is much narrower than for the boundary layer. However, in the higher Re case the value of 0.3 is reached in the boundary layer only at fairly large y^+-distances. The correlation coefficient $-\overline{u'v'}/(\overline{u'^2}\ \overline{v'^2})^{1/2}$ plotted in Fig. 7 can be seen to be much more uniform over the width of the shear layers. Of course, this coefficient drops to zero at the channel center, and it also decreases very close to the wall, but overall a value of .42 is well supported by the DNS data.

The ratio of production to dissipation of turbulent kinetic energy, P/ϵ, which

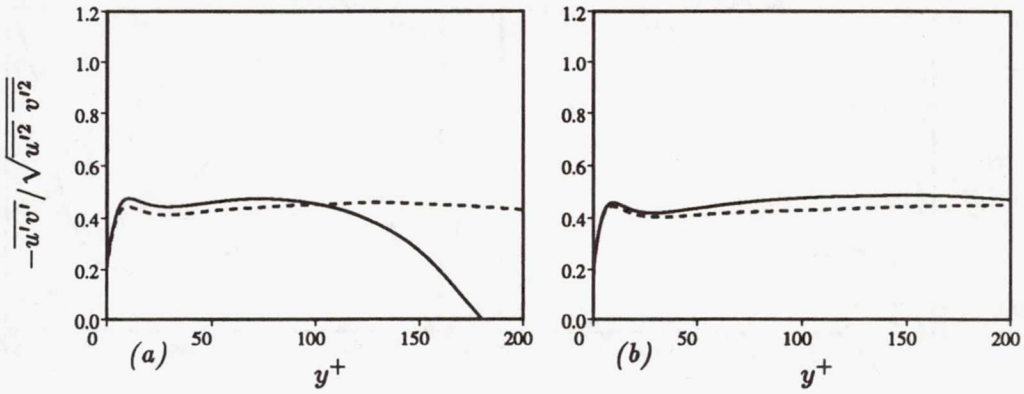

FIGURE 7. Distribution of correlation coefficient $-\overline{u'v'}/\sqrt{\overline{u'^2}\ \overline{v'^2}}$.
(a) Channel: —— $Re_\tau = 180$; ---- $Re_\tau = 395$.
(b) Boundary layer: —— $Re_\theta = 670$; ---- $Re_\theta = 1416$.

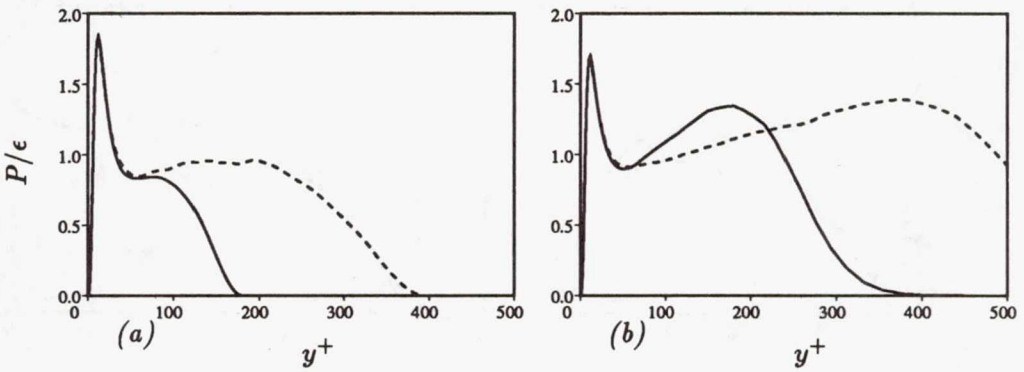

FIGURE 8. Distribution of ratio of production rate to dissipation rate of turbulent kinetic energy P/ϵ.
(a) Channel: —— $Re_\tau = 180$; ---- $Re_\tau = 395$.
(b) Boundary layer: —— $Re_\theta = 670$; ---- $Re_\theta = 1416$.

plays an important role in modeling, is given in Fig. 8. In channel flow, a substantial region with local equilibrium ($P/\epsilon \approx 1$) is present only in the higher-Reynolds number case. For the boundary-layer situation, such a region is limited to $y^+ \approx 80$ – 100, while further away from the wall, production dominates dissipation and P/ϵ reaches a maximum of about 1.4.

Finally, in Fig. 9, the ratio of turbulent to molecular viscosity, ν_t^+, is presented. The level of this quantity reached is a good indicator of the influence of viscous effects on the flow, that is whether the Reynolds number is high enough for these effects to be unimportant. Clearly the low-Re channel flow does not satisfy this criterion with ν_t^+ reaching values of only about 15. The higher-Re boundary layer reaches the highest levels of ν_t^+, as was to be expected. In the log-law region with

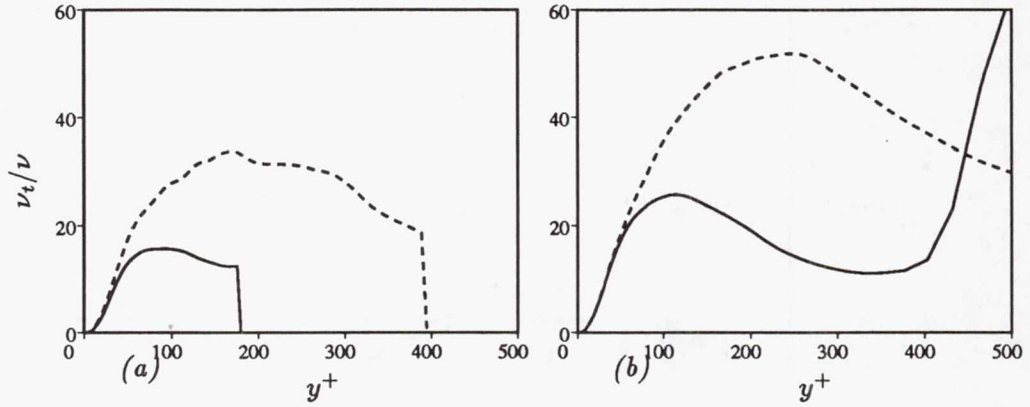

FIGURE 9. Distribution of dimensionless eddy viscosity ν_t/ν.
(a) Channel: —— $Re_\tau = 180$; ---- $Re_\tau = 395$.
(b) Boundary layer: —— $Re_\theta = 670$; ---- $Re_\theta = 1416$.

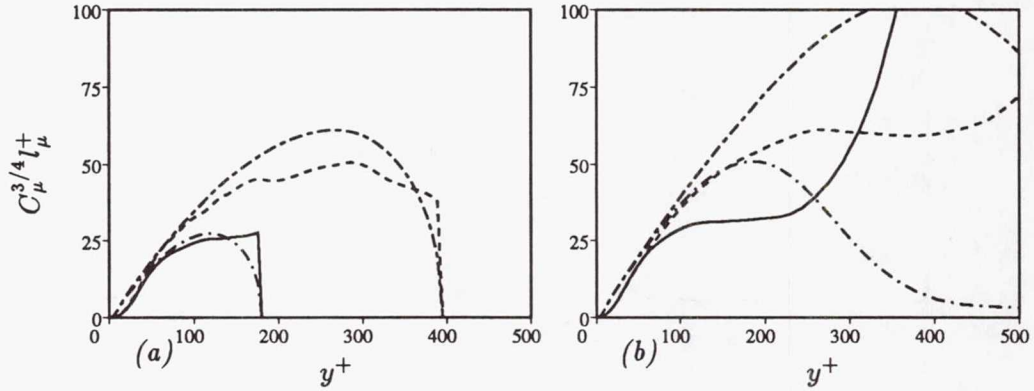

FIGURE 10. Distribution of length scale $C_\mu^{3/4} l_\mu^+$.
(a) Channel: $Re_\tau = 180$ —— DNS, —·— Eq. (11); $Re_\tau = 395$ ---- DNS, —·— Eq. (11).
(b) Boundary layer: $Re_\theta = 667$, —— DNS, —·— Eq. (11); $Re_\theta = 1416$ ---- DNS, —·— Eq. (11).

$U^+_{,y^+} = 1/\kappa y^+$, there follows from (1):

$$\nu_t^+ = -\overline{u'v'}^+ \kappa y^+ \tag{8}$$

Near the wall, ν_t^+ from the DNS data has the gradient κ, but it does not follow exactly $\nu_t^+ = \kappa y^+$ but falls below this relation because this is based on $-\overline{u'v'}^+ = 1$ while the actual shear stress is below the wall shear stress. Very near the wall, the damping of the eddy viscosity is visible, which needs to be accounted for in any turbulence model.

3. One-equation models based on $k^{1/2}$ as velocity scale

Length scale l_μ. The non-dimensional length-scale l_μ^+ defined by

$$l_\mu^+ = \frac{l_\mu U_\tau}{\nu} = \frac{\nu_t^+}{C_\mu k^{+1/2}} \tag{9}$$

was determined from the DNS data and is presented in Fig. 10. When ν_t^+ in this relation is determined from (8) based on the log law and when k^+ is assumed proportional to the shear stress $-\overline{u'v'}^+$ via

$$k^+ = \frac{-\overline{u'v'}^+}{C_\mu^{1/2}} \tag{10}$$

the following relationship for the length scale l_μ^+ results:

$$C_\mu^{3/4} l_\mu^+ = (-\overline{u'v'}^+)^{1/2} \kappa y^+ \tag{11}$$

In relation (10), $C_\mu^{1/2}$ is the structure parameter, for which a standard value of .3 has been taken so that $C_\mu = 0.09$. In Fig. 10, actually $C_\mu^{3/4} l_\mu^+$ is plotted which corresponds to the Prandtl mixing length usually assumed to be κy^+ in the log-law region. The distribution of l_μ^+ according to (11) is also included in Fig. 10. As this relation assumes the log law to hold and the structure parameter $-\overline{u'v'}/k$ to have a value of 0.3, the DNS data agree fairly well with this distribution in regions where these assumptions are approximately valid. Further away from the wall, these assumptions are not even approximately valid, so that there are considerable differences in the distributions, particularly so for the boundary layer. The differences in the curves for the various Reynolds numbers can be much reduced when l_μ/δ is plotted versus y/δ, where δ is the shear-layer thickness (channel half-width or boundary-layer thickness). $C_\mu^{3/4} l_\mu/\delta = C_\mu^{3/4} l_\mu^+ / Re_\tau$ then is approximately 0.13 in the outer region of channel flow ($y/\delta > 0.4$) and 0.095 for boundary layers in the region $.4 < y/\delta < .8$. Equation (11) can be seen to approximate the l_μ-distribution reasonably well in the near-wall region, but not too close to the wall. There, l_μ falls below the distribution (11) because of the near-wall damping of turbulent momentum transfer. A damping function à la van Driest is therefore required in this region. Fig. 11 shows the distribution of the damping function f_μ defined by

$$f_\mu = \frac{C_\mu^{3/4} l_\mu}{\kappa y} \tag{12}$$

as determined from the DNS data. f_μ is plotted versus the dimensionless wall distance y^* defined in (7), which is generally used as argument in damping functions (see equations (5) and (6)). f_μ defined by (12) following from the data does not quite reach a value of 1 as it does in models because l_μ is always below the linear

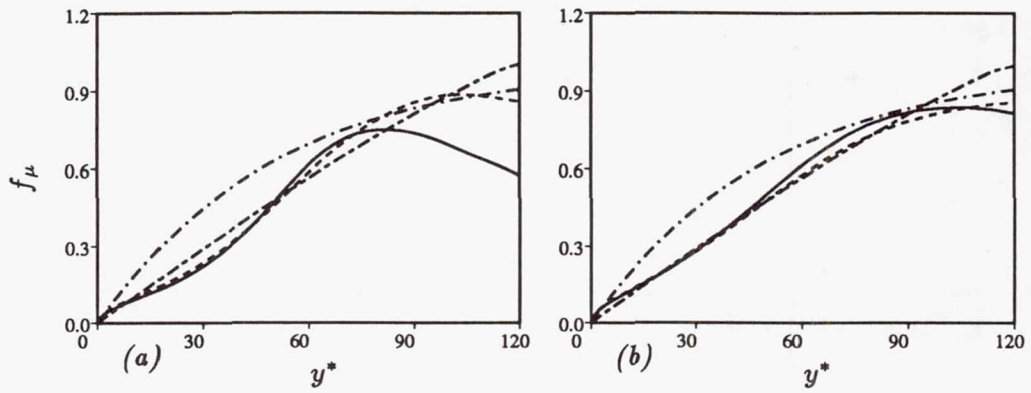

FIGURE 11. Distribution of damping function f_μ.
(a) Channel: ——— DNS $Re_\tau = 180$; - - - - DNS $Re_\tau = 395$; —·— Eq. (5) with $A_\mu^* = 50.5$; —·· Eq. (13).
(b) Boundary layer: ——— $Re_\theta = 667$; - - - - $Re_\theta = 1416$; —·— Eq. (5) with $A_\mu^* = 50.5$; —·· Eq. (13).

distribution κy (see Fig. 10). Perhaps it would be better to determine the damping function with the right-hand side of (11) in the denominator.

Commonly used exponential damping functions, *e.g.* relation (5), approach 1 further away from the wall, but they are not very accurate in the region up to $y^+ \approx 50$. An exponential function with $A_\mu^* = 50.5$ is included in Fig. 11. The DNS data are better approximated by the following power-law formula

$$f_\mu = 1 - \left(1 - \frac{y^*}{120}\right)^{1.2} \tag{13}$$

which forces f_μ to become 1 at $y^* = 120$. This relation simulates the near-wall damping quite well but approaches unity somewhat too quickly.

Dissipation length l_ϵ. The non-dimensional length scale l_ϵ^+ used for determining the dissipation rate which is defined by

$$l_\epsilon^+ = \frac{k^{+3/2}}{\epsilon^+} \tag{14}$$

is plotted in Fig. 12. When k^+ in this relation is eliminated with the aid of (10) and ϵ^+ is determined from

$$\epsilon^+ = P^+ = -\overline{u'v'}^+ U^+_{,y^+} = \frac{-\overline{u'v'}^+}{\kappa y^+} \tag{15}$$

assuming local equilibrium and the log law to hold, there results the following relation for l_ϵ^+:

$$C_\mu^{3/4} l_\epsilon^+ = (-\overline{u'v'}^+)^{1/2} \kappa y^+ \tag{16}$$

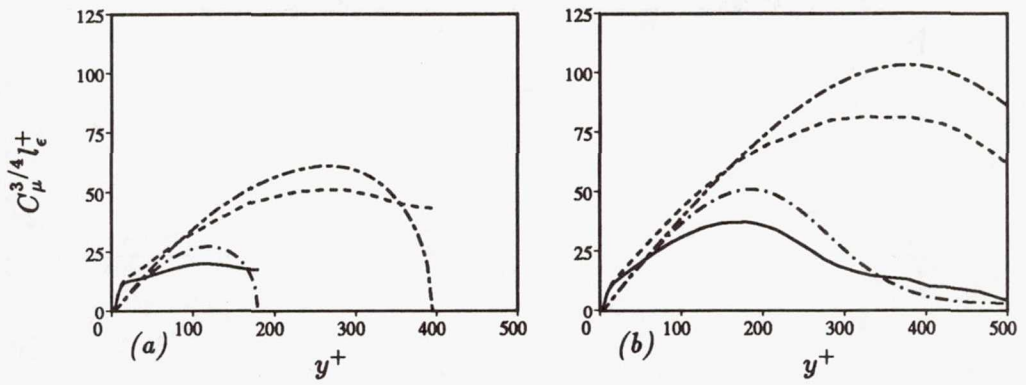

FIGURE 12. Distribution of dissipation length scale $C_\mu^{3/4} l_\epsilon^+$.
(a) Channel: $Re_\tau = 180$, —— DNS, —·— Eq. (16); $Re_\tau = 395$, ---- DNS, —·— Eq. (16).
(b) Boundary layer: $Re_\theta = 667$, —— DNS, —·— Eq. (16); $Re_\theta = 1416$, ---- DNS, —·— Eq. (16).

This is identical to relation (11) for the length scale l_μ^+ showing that, under the assumptions involved in these relations, both length scales are the same. Not too close to the wall, the behavior of l_ϵ is similar to that of l_μ, but this similarity does not extend to the channel center or the boundary-layer edge. Also, close to the wall significant differences are obvious which depend strongly on the Reynolds number. (this dependence does not disappear when l_ϵ/δ is plotted versus y/δ). A sizable region exists where l_ϵ^+ is larger than described by equation (16) or even larger than the linear relation κy^+. The maximum deviation occurs at $y^+ \approx 15$, where the distribution of the dissipation rate ϵ has a plateau (see Fig. 13). Here, existing one-equation models using a linear l_ϵ-distribution modified by a damping function according to (6) predict a peak in ϵ as shown also in Fig. 13. This ϵ-distribution with a peak away from the wall was also deduced from experiments (Patel *et al.*, 1985), but measurements of ϵ must be considered unreliable very near the wall.

As there is a considerable Reynolds-number influence on the l_ϵ-distribution, this is difficult to prescribe with a simple model relation. An alternative possibility is to introduce a model for ϵ directly via relation (15). This is plotted in Fig. 13 together with the ϵ-distribution calculated from the DNS data. It is clear that very close to the wall the behavior is very different as the right-hand side of (15) goes to zero at the wall while ϵ rises to a maximum value according to the data. Near the wall, relation (15) corresponds much closer to a modified dissipation rate $\tilde{\epsilon}$ defined by:

$$\tilde{\epsilon} = \epsilon - \nu \left(k_{,y}^{1/2} \right)^2 \tag{17}$$

In low-Reynolds-number k-ϵ models, $\tilde{\epsilon}$ is often used in the time scale k/ϵ instead of ϵ in order to keep the time scale finite at the wall. Both $\tilde{\epsilon}$ and $-\overline{u'v'}^+/\kappa y^+$ go to zero at the wall and both do so as y^2 so that relation (15) simulates correctly

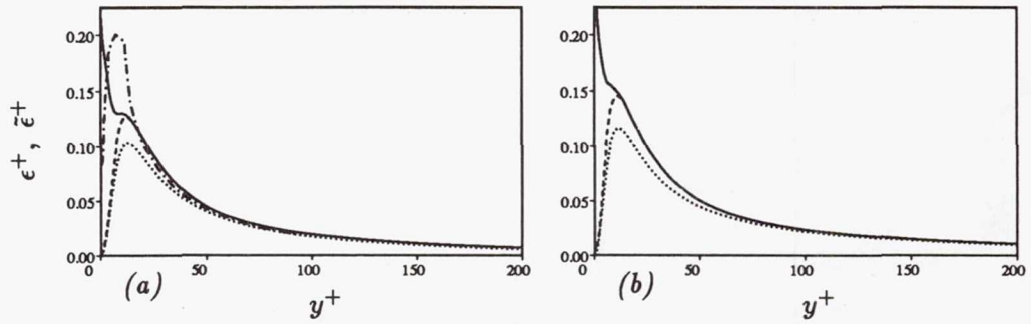

FIGURE 13. Distribution of dissipation rate ϵ^+ and $\tilde{\epsilon}^+$: —— ϵ^+; ---- $\tilde{\epsilon}^+$; ····· Eq. (15); —·— One-equation model (Cordes, 1991). *(a)* Channel, $Re = 395$. *(b)* Boundary layer, $Re_\theta = 1416$.

the behavior of $\tilde{\epsilon}$ near the wall. Relation (15) is based on the assumption of local equilibrium and on the validity of the logarithmic velocity distribution and can be seen to be a reasonably good approximation to ϵ in the y^+-range 100 – 200. However, in the case of the boundary layer deviations already increase at the larger y^+-values in this range as the velocity profile starts to deviate from the logarithmic distribution (see Fig. 2). Closer to the wall, $\tilde{\epsilon}$ (which is different from ϵ only for $y^+ \leq 12$) is also quite well simulated by (15), particularly so the shape. The peak, however, is predicted somewhat too low. In this region, the actual velocity gradient is larger than $1/\kappa y^+$, but dissipation is smaller than production (see Fig. 8). These two influences compensate each other to a large extent, but not 100% so that $\tilde{\epsilon}$ is somewhat underpredicted. A pragmatic approach to the simulation of $\tilde{\epsilon}$ is to multiply the right-hand side of relation (15) by a factor of about 1.2 which then yields $\tilde{\epsilon}$-distributions which are approximately correct for all cases considered here.

4. One-equation model based on $(\overline{v'^2})^{1/2}$ as velocity scale

Durbin (1990) suggested that, in near-wall shear layers, the normal fluctuations $(\overline{v'^2})^{1/2}$ may be a better velocity scale for characterizing the turbulent motion than $k^{1/2}$ and that no damping functions may be needed when this velocity scale is used. Hence, it is intriguing to examine whether this choice of velocity scale leads to corresponding length scales which are easier to prescribe empirically. Of course, the question then also needs to be answered as to how $\overline{v'^2}$ can be related to other known quantities in the context of a one-equation model.

Length-scale $l_{\mu,v}$. When $k^{1/2}$ is replaced by $(\overline{v'^2})^{1/2}$ in the eddy-viscosity relation (2), there follows:

$$\nu_t = (\overline{v'^2})^{1/2} l_{\mu,v} \tag{18}$$

It should be noted that any constant that may occur has been absorbed in $l_{\mu,v}$. In Fig. 14, the distribution of the dimensionless length scale $l^+_{\mu,v}$ as determined from the DNS data is compared with the distribution from the following approximate

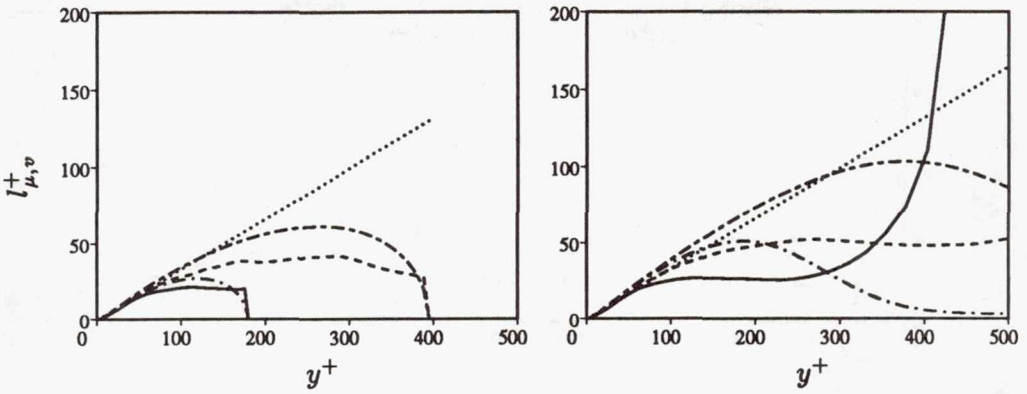

FIGURE 14. Distribution of length scale $l^+_{\mu,v}$: ····· Eq. (20).
(a) Channel: $Re_\tau = 180$, —— DNS, —·— Eq. (19); $Re_\tau = 395$, ---- DNS, —·— Eq. (19).
(b) Boundary layer: $Re_\theta = 667$, —— DNS, —·— Eq. (19); $Re_\theta = 1416$, ---- DNS, —·— Eq. (19).

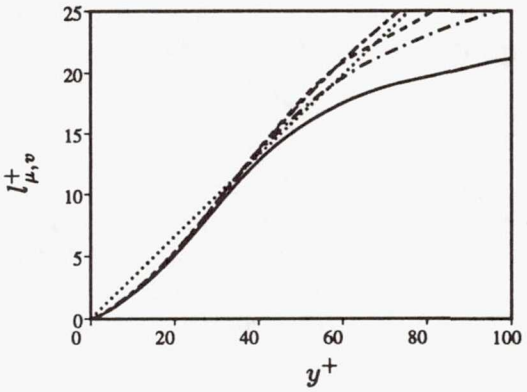

FIGURE 15. Distribution of length scale $l^+_{\mu,v}$, near the wall: ····· Eq. (20); —— Channel $Re_\tau = 180$; ---- Channel $Re_\tau = 395$; —·— Boundary layer $Re_\theta = 667$; —·— Boundary layer $Re_\theta = 1416$.

formula:

$$l^+_{\mu,v} = \frac{\nu_t^+}{(\overline{v'^2}^+)^{1/2}} = \frac{-\overline{u'v'}^+ \kappa y^+}{(\overline{v'^2}^+)^{1/2}} \tag{19}$$

This formula is again obtained by replacing the eddy viscosity by relation (7) based on the log law. Further, it can be seen from Fig. 3 that $\overline{v'^2}^+$ is approximately 1, and this value was inserted in relation (19) for the curve shown in Fig. 14. The figure indicates that, for larger y^+-values, the DNS data deviate more from the approximation curve than in the case of l_μ (see Fig. 10). However, close the wall ($y^+ < 60$) the data follow much closer the approximate relation, which is virtually

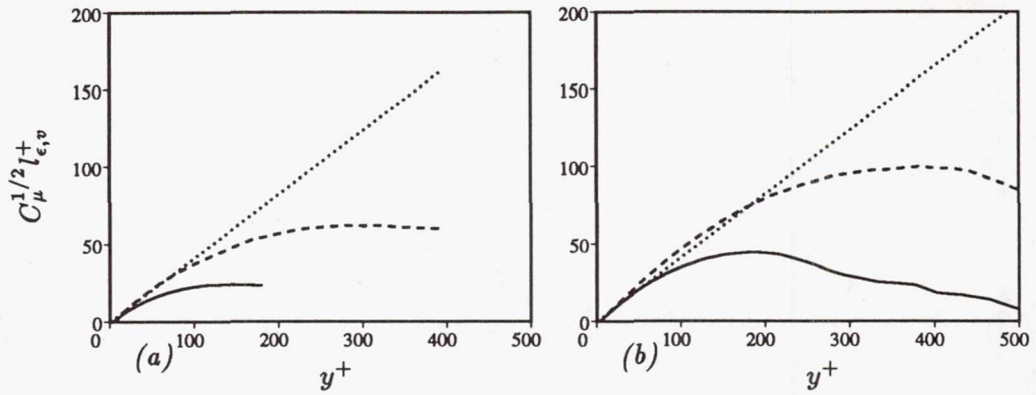

FIGURE 16. Distribution of dissipation length $C^{1/2}l^+_{\epsilon,v}$: ····· κy^+;
(a) Channel;—— $Re_\tau = 180$;---- $Re_\tau = 395$.
(b) Boundary layer; —— $Re_\theta = 667$; ---- $Re_\theta = 1416$.

linear in this region. Hence there is considerably less damping than in the case of l_μ. This is due to the fact that $\overline{v'^2}/k$ decreases near the wall (see Fig. 5) and that right at the wall $l_{\mu,v} \propto y$ while $l_\mu \propto y^2$. There appears to be some damping, but to first approximation the data can be described by

$$l_{\mu,v} = C_{l,\mu} y \tag{20}$$

where the factor $C_{l,\mu}$ is somewhat smaller than κ. As can be seen from Fig. 15, the linear distribution with $C_{l,\mu} = 0.33$ approximates the data fairly well up to $y^+ \approx 60$. It may be also of interest that $l_{\mu,v}/\delta = l^+_{\mu,v}/Re_\tau$ is approximately 0.12 in the outer part of channel flow and 0.08 in boundary-layer regions with $.4 < y/\delta < .8$.

Dissipation length $l_{\epsilon,v}$. When $(\overline{v'^2})^{1/2}$ is used as velocity scale, the dissipation relation corresponding to (4) reads:

$$\epsilon = \frac{(\overline{v'^2})^{1/2} k}{l_{\epsilon,v}} \tag{21}$$

which is practically a relation between a velocity scale, a length scale and the time scale k/ϵ. The dimensionless length scale $l^+_{\epsilon,v}$ can be approximated as

$$l^+_{\epsilon,v} = \frac{k^+}{\epsilon^+}(\overline{v'^2}^+)^{1/2} = \frac{1}{C_\mu^{1/2}} \kappa y^+ (\overline{v'^2}^+)^{1/2} \tag{22}$$

which again results from the elimination of k^+ with the aid of (10) and of ϵ^+ with the aid of (15), involving local-equilibrium and log-law assumptions. In Fig. 16, $C_\mu^{1/2} l^+_{\epsilon,v}$ determined from the DNS data is plotted together with the line κy^+ resulting from (22) by assuming again that $\overline{v'^2}^+$ has a value of 1. Fig. 16 shows that this linear relation approximates the channel flow data near the wall very well, while the data

indicate a somewhat larger slope for the boundary layer. This is due to the fact that in the boundary layer $\overline{v'^2}^+$ is somewhat larger than 1 in the region considered (see Fig. 3). Further, the lower-Reynolds-number cases follow the linear distribution only up to rather small y^+-values. In the bulk of the flow at larger y^+ distances, constant values of $l^+_{\epsilon,v}$ are approached. When $l^+_{\epsilon,v}$ is made dimensionless with δ, $C_\mu^{1/2} l_{\epsilon,v}/\delta \approx 0.14$ for both channel and boundary layer flows. Near the wall, the following linear distribution can be recommended:

$$l_{\epsilon,v} = C_{l,\epsilon} y \tag{23}$$

with $C_{l,\epsilon} \approx 1.43$ as an average value. This linear relation is a reasonable approximation up to $y/\delta \approx 0.2$.

Determination of $\overline{v'^2}$. When $(\overline{v'^2})^{1/2}$ is used as velocity scale in the turbulence model, the distribution of $\overline{v'^2}$ needs to be determined. The most direct way to obtain $\overline{v'^2}$ would be to solve a transport equation for $\overline{v'^2}$ and this is what Durbin (1990) proposed when he introduced $(\overline{v'^2})^{1/2}$ as velocity scale. However, the pressure-strain term in the $\overline{v'^2}$-equation has then to be modeled and, especially for near-wall regions, this is a difficult and an unresolved problem. Further, for a simple near-wall model for use in practical calculations, it is desirable to keep the model at the one-equation level and not to add further equations. Hence, the suggestion of Hanjalić and Launder (1976) is followed here to introduce a simple relation between $\overline{v'^2}/k$ and $\overline{u'v'}/k$. Hanjalić and Launder based their simple relation on two assumptions. First, they assumed that the shear-stress correlation coefficient is constant, *i.e.*

$$\frac{-\overline{u'v'}}{(\overline{u'^2}\ \overline{v'^2})^{1/2}} = \text{constant} \tag{24}$$

They further assumed that the kinetic energy is related to the components $\overline{u'^2}$ and $\overline{v'^2}$ by

$$k = a(\overline{u'^2} + \overline{v'^2}) \tag{25}$$

where a is a constant, which also implies that the ratio $\overline{w'^2}/k = \text{constant}$. The first assumption is well supported by the DNS data, as can be seen from Fig. 7. Fig. 5 shows that the second assumption is also well supported away from the wall while near the wall $\overline{w'^2}/k$ has a dip which however recovers at the wall itself. This dip is stronger in the channel flow than in the boundary layer. Combining relations (24) and (25) yields:

$$\frac{\overline{v'^2}}{k} = \frac{a}{c^2}\left(\frac{\overline{u'v'}}{k}\right)^2 + a\left(\frac{\overline{v'^2}}{k}\right)^2 \tag{26}$$

which is a quadratic equation for $\overline{v'^2}/k$. Hanjalić and Launder (1976) linearized this equation by omitting the second term on the right-hand side and compensating for this by suitably choosing the coefficient in front of the first term. Their final model relation reads:

$$\frac{\overline{v'^2}}{k} = 4\left(\frac{\overline{u'v'}}{k}\right)^2 \tag{27}$$

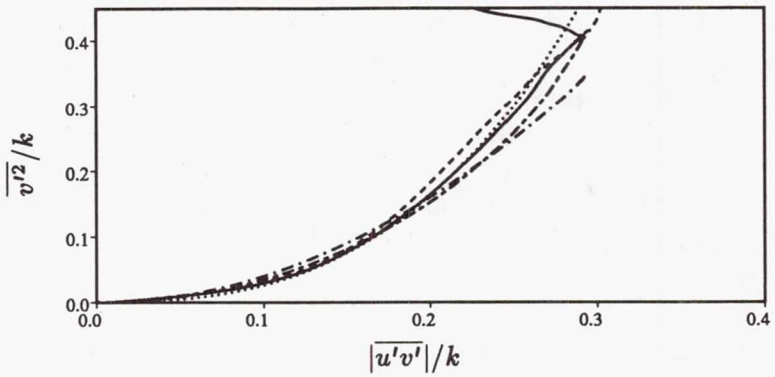

FIGURE 17. Variation of $\overline{v'^2}/k$ versus $|\overline{u'v'}|/k$: —— channel DNS $Re_\tau = 395$; ---- Boundary layer DNS $Re_\theta = 1416$; —·— Eq. (27); —··— Eq. (28); ····· Eq. (29).

This relation is compared in Fig. 17 with the DNS data and shows that altogether it is not a bad fit but underpredicts $\overline{v'^2}/k$ as $\overline{u'v'}/k$ approaches 0.3. When the quadratic equation (26) is solved for $\overline{v'^2}/k$, there results:

$$\frac{\overline{v'^2}}{k} = \frac{1}{2a}\left(1 - \sqrt{1 - 4\left(\frac{a}{c}\right)^2\left(\frac{\overline{u'v'}}{k}\right)^2}\right) \tag{28}$$

With $a = 0.7$ and $c = 0.42$ as a consensus of the data (see Figs. 5 and 7) the resulting curve is also included in Fig. 17. This provides a better fit at the larger $\overline{u'v'}/k$-values, but the relation still underpredicts $\overline{v'^2}/k$ in the range $.2 < |\overline{u'v'}|/k < .25$. A better representation over the entire range of $\overline{u'v'}/k$ can be obtained by the following fit to the data:

$$\frac{\overline{v'^2}}{k} = 1.13\left(\frac{\overline{u'v'}}{k}\right)^2 + 14.67\left(\frac{|\overline{u'v'}|}{k}\right)^3 \tag{29}$$

This curve is also included in Fig. 17 and can be seen to represent the relation between $\overline{v'^2}/k$ and $\overline{u'v'}/k$ with sufficient accuracy for use in a one-equation model restricted to the near-wall region.

5. Conclusions

The direct simulation data have shown that, for the Reynolds number investigated, there is still considerable influence of the Reynolds number on the quantities plotted in wall coordinates. However, for the higher Reynolds numbers simulated, the quantities are already close to those observed in experiments at much higher Reynolds numbers. On the other hand, for both channel and boundary layer the lower-Reynolds-number cases are subject to considerable viscous effects. It was also found that, except very close to the wall, the normal stresses are somewhat higher in boundary-layer than in channel flow because of the different shear-stress behavior.

The length scale l_μ in the eddy-viscosity relation of existing one-equation models follows a near-linear behavior near the wall, but very close to the wall it falls below this distribution and requires the introduction of a damping function similar to that for the mixing-length distribution. Damping functions were evaluated with the aid of the DNS data, and the existing ones were found not to be accurate. Based on the data, a new damping function was proposed. The distribution of the length scale l_ϵ in the dissipation relation shows a pronounced hump at $y^+ \approx 15$ and lies considerably above the linear distribution near the wall. This behavior is not easy to describe in a simple relation, but the distribution of the modified dissipation rate $\tilde{\epsilon}$ itself can be fairly accurately modeled in terms of shear stress and wall distance.

When the normal fluctuations $(\overline{v'^2})^{1/2}$ are introduced as velocity scale instead of $k^{1/2}$, the corresponding length scales are better behaved, *i.e.* the dissipation length $l_{\epsilon,v}$ does not have a hump and the length $l_{\mu,v}$ is subject to much less damping. Near the wall, both length scales can be approximated quite well by linear relations and no damping functions are needed. It was found that $\overline{v'^2}/k$ and $\overline{u'v'}/k$ correlate quite well near the wall, and a correlation was proposed for use in one-equation models which avoids solving an additional equation of $\overline{v'^2}$. Together with the length-scale relations introduced this forms a new one-equation model which should now be tested in actual flow calculations.

The authors are grateful to Dr. Kim for providing the unpublished direct simulation data for the channel flow at $Re_\tau = 395$. The first author (WR) would like to acknowledge the generous support of the Center for Turbulence Research.

REFERENCES

CLARK, J. A. 1968 A study of incompressible turbulent boundary layers in channel flow. *ASME J. Basic Eng.* **90**, 455-468.

CORDES, J. 1991 Entwicklung und Anwendung eines Zweischichten-Turbulenzmodells für abgelöste dreidimensionale Strömungen. *Ph.D. Thesis,* University of Karlsruhe.

DURBIN, P. A. 1990 Near-wall turbulence closure modeling without "damping functions". *CTR Manuscript 112,* Center for Turbulence Research, Stanford University.

HANJALIĆ, K. & LAUNDER, B. E. 1976 Contribution towards a Reynolds-stress closure for low-Reynolds-number turbulence. *J. Fluid Mech.* **74**, 593-610.

HUSSAIN, A. K. M. F. & REYNOLDS, W. C. 1975 Measurement of fully developed turbulent channel flow. *ASME J. Fluids Eng.* **97**, 568-580.

KASTRINAKIS, E. G. & ECKELMANN, H. 1983 Measurement of streamwise vorticity fluctuations in a turbulent channel flow. *J. Fluid Mech.* **137**, 165-186.

KIM, J. 1990 private communication.

KIM, J., MOIN, P. & MOSER, R. 1987 Turbulence statistics in fully developed channel flow at low Reynolds number. *J. Fluid Mech.* **177**, 133-166.

LAUFER, J. 1954 The structure of turbulence in fully developed pipe flow. *NACA Rept. 1174.*

MYONG, H. K. & KASAGI, N. 1988 An anisotropic k-ϵ model taking into account the near-wall limiting behavior of turbulence. Proc. 20th Turbulence Symposium, Tokyo.

NORRIS, L. H. & REYNOLDS, W. C. 1975 Turbulent channel flow with a moving wavy boundary. *Rept. No. FM-10,* Stanford University, Dept. of Mech. Eng.

PATEL, V. C., RODI, W. & SCHEUERER, G. 1985 Turbulence models for near-wall and low-Reynolds number closure: A review. *AIAA J.* **23**(9), 1308-1319.

RODI, W. 1991 Experience with two-layer models combining the k-ϵ model with a one-equation model near the wall. *paper AIAA 91-0216,* Reno, 1991.

SPALART, P. R. 1988 Direct simulation of a turbulent boundary layer up to $R_\theta = 1410$. *J. Fluid Mech.* **187**, 61-98.

WOLFSHTEIN, M. 1969 The velocity and temperature distribution in one-dimensional flow with turbulence augmentation and pressure gradient. *Int. J. Heat Mass Transfer.* **12**, 301-118.